Acta Cryst. (1977). A33, 390–395

Improvement of Alignment in Diffuse Fibre Diffraction Patterns

BY R. LOVELL AND A. H. WINDLE

Department of Metallurgy and Materials Science, University of Cambridge, Pembroke Street, Cambridge CB2 3QZ

(*Received* 25 *October* 1976; *accepted* 15 *November* 1976)

Molecular alignment of crystalline polymers leads to 'fibre type' X-ray diffraction patterns which are a rich source of structural information. For aligned glassy polymers, however, it is only possible to obtain a very diffuse fibre pattern. This paper describes a technique developed to improve the alignment of such patterns by azimuthal sharpening. The technique is based on consideration of the contribution to the diffraction pattern due to scattering from a fibre entity oriented at an angle to the specimen's extension axis. The distribution of these entities about the specimen axis is determined from the azimuthal profile of a diffuse diffraction halo which has concentrated on the equator of the pattern. Integral equations are developed which describe the appearance of a smeared reflexion on the diffraction pattern in terms of the entity distribution. Solution of these equations by an iterative procedure enables the diffraction pattern to be azimuthally sharpened. The result is a diffuse version of a typical fibre pattern, which is useful in the prediction of chain conformation and packing as well as levels of disorder present.

1. Introduction

As part of an investigation of the structure of glassy polymers, we have measured wide-angle X-ray diffraction patterns from specimens aligned by drawing at temperatures just below their glass transitions (Lovell & Windle, 1976; Colebrooke & Windle, 1976). The measurements were made with the symmetric transmission arrangement (Fig. 1), the specimen being rotated in its own plane (*i.e.* about the y axis) for each value of $2\theta_B$. The diffracted intensity is plotted as contour maps with $s=(4\pi \sin \theta_B/\lambda)$ measured radially and ψ measured azimuthally from the equator (Fig. 2). Owing to the lack of perfect alignment, the diffuse spots that would be expected if the only disorder were from paracrystallinity and small crystal size have been azimuthally smeared into diffuse arcs.

In this paper we describe in detail a technique developed to remove the component of azimuthal smearing from the experimental intensity $I(s,\psi)$ to give a pattern that may be viewed as a diffuse example of the familiar crystalline fibre pattern.

Examples of the application of this technique to aligned glassy polymers have already been presented (Lovell & Windle, 1976).

The paper is organized as follows. We first assume a model of an aligned glassy polymer consisting of diffracting entities with fibre symmetry. Next we consider how the diffraction pattern of a single aligned entity is altered when the entity is rotated to a general orientation. The effect on the equatorial intensity is simple and this enables us to measure the distribution of entity axes. We make the approximation that the distribution can be built up in two stages: spreading in the plane that includes the extension direction and the y' axis, followed by rotation about the y' axis. Azimuthal sharpening is then carried out by reversing these two stages to obtain the diffraction pattern of a single entity.

2. Diffraction from a single fibre entity

The specimens used have fibre symmetry about the extension direction (z' axis) and we consider them to be composed of identical diffracting entities each with its own fibre symmetry. The distribution of the fibre axes of these entities about the extension direction, $\Phi(\alpha)$, may be shown on a pole figure (Fig. 3). The individual diffracting domains may not have fibre symmetry. However, we group together all domains that share a common molecular orientation, irrespective of their location in the specimen, to create a 'fibre entity' which does possess fibre symmetry.

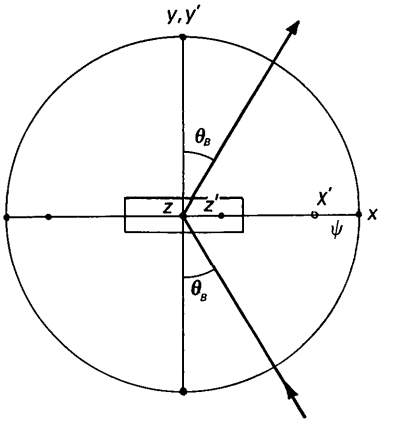

Fig. 1. Incident and diffracted beams superimposed on a stereographic projection of axes defining the experimental geometry (xyz) and the specimen axes ($x'y'z'$). The extension direction is z' and the normal to the 'reflexion plane', y, y'.

Each fibre entity will contribute to the diffraction pattern according to its angular position in relation to the extension direction. A change in orientation of an entity can change both the intensity and the azimuthal position (ψ) of a 'reflexion' but not its value of s. For the present work, the orientation of the axis of an entity is specified by polar coordinates referred to the y' axis of the specimen, *i.e.* a rotation of α_1 about the x' axis followed by a rotation of α_2 about the y' axis as shown in the stereographic projection of Fig. 4. The effect of these two rotations on a sharp reflexion will now be derived.

2.1. *Rotation* α_1

Fig. 5 shows the construction in reciprocal space for calculating the position of a reflexion at an angle ψ' to the equator of the entity. In reciprocal space, this reflexion is derived from the intersection of the

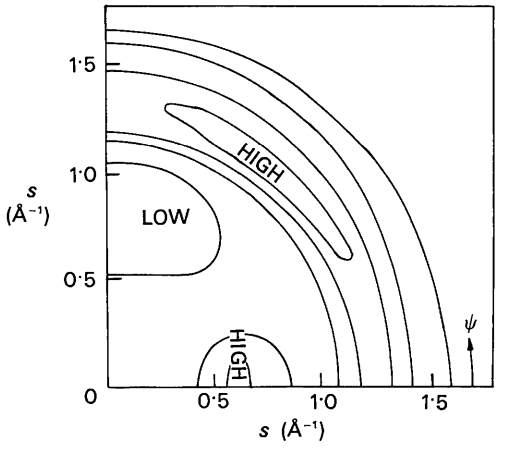

Fig. 2. Plot of uncorrected diffracted intensity from an aligned specimen of glassy isotactic polystyrene (Lovell & Windle, 1976). The intensity is in arbitrary units and the contours are at equal intervals.

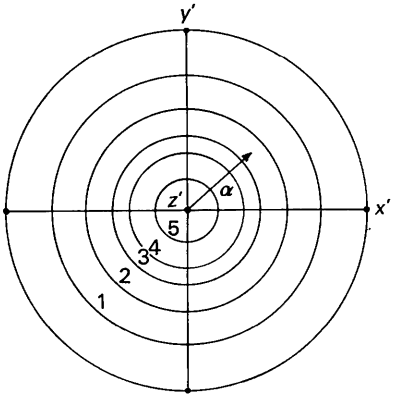

Fig. 3. Pole figure illustrating distribution of fibre axes around the z' axis.

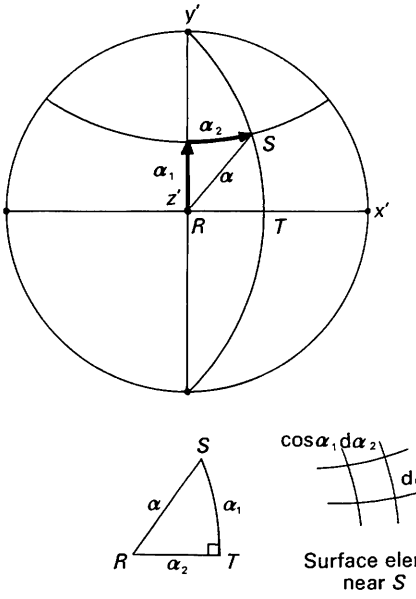

Fig. 4. Steoreographic projection based on specimen axes ($x'y'z'$) illustrating the polar coordinate system to define the orientation of the fibre entity at S.

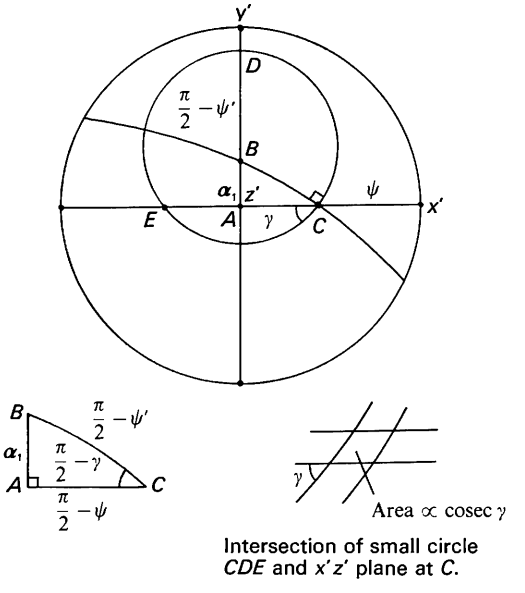

Fig. 5. Stereographic projection showing the locus of a reflexion (the small circle, centre B) at an angle ψ' to the equator of an entity tilted away from the z' axis by α_1 about x'.

small circle (CDE) and the 'reflexion plane' ($x'z'$ plane) at C. The integrated intensity of the reflexion is proportional to the area of the intersection (see inset in Fig. 5) and hence is proportional to cosec γ. If the axis of the entity is at an angle α_1 from the z' axis in the $y'z'$ plane, then the reflexion will appear at an azimuthal angle ψ ($\geq\psi'$) (Fig. 6*a*) and its integrated intensity $\mathscr{I}_0$ will be increased to $\mathscr{I}_0$ cosec γ.

From the spherical triangle ABC in Fig. 5 we obtain

$$\sin\psi' = \sin\psi\cos\alpha_1\,, \tag{1}$$

$$\cos\alpha_1 = \sin\psi'\sin\psi + \cos\psi'\cos\psi\sin\gamma\,. \tag{2}$$

Hence

$$\sin\psi = \frac{\sin\psi'}{\cos\alpha_1} \quad \text{for} \quad \alpha_1 \le \frac{\pi}{2} - \psi'\,, \tag{3}$$

$$\mathscr{I}_1 = \mathscr{I}_0 \operatorname{cosec}\gamma = \frac{\mathscr{I}_0\cos\psi'}{(\cos^2\alpha_1 - \sin^2\psi')^{1/2}}\,. \tag{4}$$

Since $\sin\psi$ cannot be greater than one, all reflexions for which $\psi' > \pi/2 - \alpha_1$ will disappear (*i.e.* the small circle will no longer intersect the 'reflexion plane').

2.1.1. *Special reflexions*

(*a*) *Equatorial* ($\psi' = 0$). Rotation α_1 merely changes the intensity; (3) and (4) become

$$\psi = \psi' = 0 \tag{5}$$

$$\mathscr{I}_1 = \mathscr{I}_0 \sec\alpha_1\,. \tag{6}$$

(*b*) *Meridional* ($\psi' = \pi/2$). Rotation α_1 ($\neq 0$) makes the diffraction spot disappear since (3) gives $\sin\psi$ greater than one. Hence only an entity with $\alpha_1 = 0$ can contribute its meridional intensity to the diffraction pattern.

2.2. *Rotation* α_2

All reflexions are moved around the ring of constant s on the diffraction pattern by an angle α_2, without change of intensity (Fig. 6*b*).

3. Diffraction from a distribution of fibre entities

We now consider a general distribution of entity axes $\Phi(\alpha_1,\alpha_2)$ which does not necessarily possess fibre symmetry about the extension direction. The probability of an entity axis lying between (α_1,α_2) and $(\alpha_1+\mathrm{d}\alpha_1, \alpha_2+\mathrm{d}\alpha_2)$ is given by:

$$\Phi(\alpha_1,\alpha_2)\cos\alpha_1\mathrm{d}\alpha_1\mathrm{d}\alpha_2 \tag{7}$$

where

$$\int_{-\pi/2}^{\pi/2}\int_{-\pi/2}^{\pi/2}\Phi(\alpha_1,\alpha_2)\cos\alpha_1\mathrm{d}\alpha_1\mathrm{d}\alpha_2 = 1$$

(see surface element in Fig. 4).

The projection of this distribution on the $y'z'$ plane, $D_1(\alpha_1)$, is given by:

$$D_1(\alpha_1) = \cos\alpha_1\int_{-\pi/2}^{\pi/2}\Phi(\alpha_1,\alpha_2)\mathrm{d}\alpha_2 \tag{7a}$$

where

$$\int_{-\pi/2}^{\pi/2} D_1(\alpha_1)\mathrm{d}\alpha_1 = 1\,.$$

The distribution function $\Phi(\alpha_1,\alpha_2)$ has the effect of azimuthally smearing the features on a diffraction pattern characteristic of a single entity. For a feature in a general position, the nature of the smearing will be described by a complicated double integral. However, in the special case of equatorial and meridional features, the integral reduces to a more manageable form.

(*a*) *Equatorial.* The azimuthal spread of an equatorial feature is essentially the projection of $\Phi(\alpha_1,\alpha_2)$ onto the $x'z'$ plane. However, the contribution of the equatorial scattering of an entity to the recorded diffraction pattern depends on $\sec\alpha_1$ (6). Hence:

$$I_{\mathrm{eq}}(\alpha_2) \propto \int_{-\pi/2}^{\pi/2}\Phi(\alpha_1,\alpha_2)\cos\alpha_1\sec\alpha_1\mathrm{d}\alpha_1 = \int_{-\pi/2}^{\pi/2}\Phi(\alpha_1,\alpha_2)\mathrm{d}\alpha_1. \tag{8}$$

(*b*) *Meridional.* The meridional scattering of a single entity can only contribute to the diffraction pattern when $\alpha_1 = 0$. Hence:

$$I_{\mathrm{mer}}(\alpha_2) \propto \Phi(0,\alpha_2)\,. \tag{9}$$

This is the section of $\Phi(\alpha_1,\alpha_2)$ made by the $x'z'$ plane.

4. Fibre symmetry

So far we have dealt with a general distribution. In a specimen with fibre symmetry, the distribution can

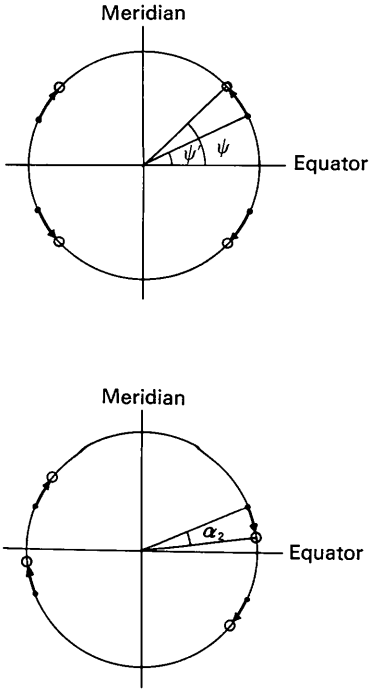

Fig. 6. The effect of (*a*) rotation of an entity by α_1 about x', and (*b*) rotation by α_2 about y', on the azimuthal position of a reflexion which is at ψ' to the equator of the entity.

only depend on the angle between the entity axis and the extension direction (*i.e.* the angle α in Fig. 4). Hence we can write

$$\Phi(\alpha_1,\alpha_2)=\Phi_1(\alpha)=\Phi_2(\cos\alpha) \qquad (10a)$$

where

$$2\pi\int_0^{\pi/2}\Phi_2(\cos\alpha)\sin\alpha\,d\alpha=1.$$

Now, from the spherical triangle RST in Fig. 4:

$$\cos\alpha=\cos\alpha_1\cos\alpha_2$$

and thus

$$\Phi(\alpha_1,\alpha_2)=\Phi_2(\cos\alpha_1\cos\alpha_2)\,. \qquad (10b)$$

In this case, (7*a*) and (8) become:

$$D_1(\alpha_1)=\cos\alpha_1\int_{-\pi/2}^{\pi/2}\Phi_2(\cos\alpha_1\cos\alpha_2)d\alpha_2 \qquad (11)$$

and

$$I_{eq}(\alpha_2)\propto\int_{-\pi/2}^{\pi/2}\Phi_2(\cos\alpha_1\cos\alpha_2)d\alpha_1\,. \qquad (12)$$

However, because Φ_2 is a function of the product $\cos\alpha_1\cos\alpha_2$, it is possible to interchange α_1 and α_2 in equation (12) giving:

$$I_{eq}(\alpha_1)\propto\int_{-\pi/2}^{\pi/2}\Phi_2(\cos\alpha_1\cos\alpha_2)d\alpha_2 \qquad (13)$$

and hence:

$$D_1(\alpha_1)\propto(\cos\alpha_1)I_{eq}(\alpha_1)\,, \qquad (14)$$

i.e. the projection of the distribution on the $y'z'$ plane is proportional to the azimuthal profile of the equatorial halo multiplied by $\cos\alpha_1$.

Thus, provided we can assume that poor orientation is the main cause of azimuthal smearing, a well separated equatorial arc gives a measure of the orientation distribution. In determining this, we view the diffraction pattern as the sum of two components, one due to randomly oriented entities and hence having uniform halos, the other due to the entities that produce the overall texture. For this second component, the azimuthal profile of an equatorial halo will have a minimum value of zero.

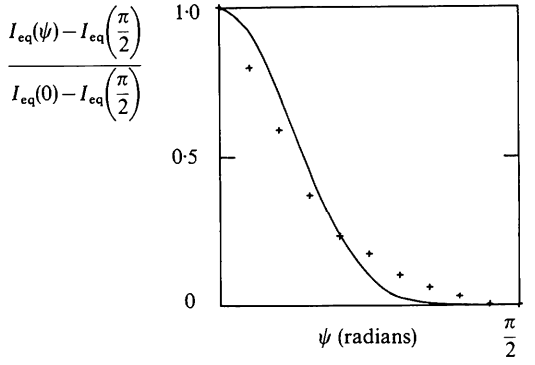

Fig. 7. Plot of the azimuthal profile of an equatorial reflexion for glassy isotactic polystyrene (+) compared with the function $\cos^7\psi$.

5. Simplified distribution – two-stage construction

In order to simplify the sharpening procedure, we now make the assumption that the distribution may be expressed as a product:

$$\Phi_2(\cos\alpha)=\frac{\Phi_2(\cos\alpha_1)\Phi_2(\cos\alpha_2)}{\Phi_2(0)}. \qquad (15)$$

This requires, in fact, that the distribution be of the form [with the use of equation (10*a*)]:

$$\Phi_2(\cos\alpha)=\frac{(k+1)}{2\pi}\cos^k\alpha \qquad (16)$$

where k is positive and, from equation (12),

$$I_{eq}(\psi)\propto\cos^k\psi\,. \qquad (17)$$

To test the validity of the assumption of (15), for diffraction from aligned glassy polymers, we have fitted a function of the form $\cos^k\psi$ to the azimuthal profile of the equatorial halo of glassy isotactic polystyrene. Fig. 7 demonstrates reasonable agreement when $k=7$. The fit may not of course be at all acceptable with different materials, particularly in the case of two-component systems where one component is much better oriented than the other.

The reason for requiring the distribution to be expressible as a product is that we may then consider it to be constructed in two stages: (i) the entity axes are first distributed in the $y'z'$ plane (about the x' axis) according to $D_1(\alpha_1)$; (ii) they are then distributed about the y' axis according to $\Phi_2(\cos\alpha_2)$, with $\Phi_2(\cos\alpha_2)$ being independent of α_1.

For any given value of s, we now define three azimuthal intensity profiles representing the stages by which the smearing is removed: $I_1(\psi)$ for entities distributed as $\Phi_2(\cos\alpha)$, *i.e.* the full distribution; $I_2(\psi)$ for entities distributed as $D_1(\alpha_1)$ in the $y'z'$ plane; $I(\psi)$ for all entities aligned parallel to the z' axis.

Now, from (3), intensity at ψ' to the equator of an entity will only appear at $\psi(\geq\psi')$ in the diffraction pattern if the entity axis is tilted in the $y'z'$ plane at an angle α_1 given by

$$\cos\alpha_1=\frac{\sin\psi'}{\sin\psi}\,. \qquad (18)$$

Hence, the distribution $D_1(\alpha_1)$ in the $y'z'$ plane will smear intensity at ψ' to higher azimuthal angles according to the function:

$$2D_1\left[\alpha_1=\cos^{-1}\left(\frac{\sin\psi'}{\sin\psi}\right)\right]\times\left|\frac{d\alpha_1}{d\psi}\right|\times\frac{\cos\psi'}{(\cos^2\alpha_1-\sin^2\psi')^{1/2}}\,. \qquad (19)$$

The first two terms of this function are the distribu-

tion of ψ derived from $D_1(\alpha_1)$ by using (18). The third term is the geometric intensity factor of (4).

Substituting $\cos\alpha_1$ from (18) into the intensity factor gives

$$\frac{\cos\psi'}{(\cos^2\alpha_1-\sin^2\psi')^{1/2}}=\frac{\tan\psi}{\tan\psi'}, \tag{20}$$

and differentiating (18) gives:

$$\frac{d\alpha_1}{d\psi}=\frac{\cos\psi\sin\psi'}{\sin\psi(\sin^2\psi-\sin^2\psi')^{1/2}}. \tag{21}$$

Hence, expressed in terms of ψ and ψ', the function (19) becomes

$$2D_1\left[\cos^{-1}\left(\frac{\sin\psi'}{\sin\psi}\right)\right]\times\frac{\cos\psi\sin\psi'}{\sin\psi(\sin^2\psi-\sin^2\psi')^{1/2}}\times\frac{\tan\psi}{\tan\psi'} \tag{22}$$

which was derived as function (8) in our earlier paper (Lovell & Windle, 1976).

This simplifies to

$$2D_1\left[\cos^{-1}\left(\frac{\sin\psi'}{\sin\psi}\right)\right]\frac{\cos\psi'}{(\sin^2\psi-\sin^2\psi')^{1/2}} \tag{23}$$

which smears the intensity distribution of an entity $I(\psi')$ according to the integral

$$I_2(\psi)=2\int_0^{\psi}I(\psi')D_1\left[\cos^{-1}\left(\frac{\sin\psi'}{\sin\psi}\right)\right]\times\frac{\cos\psi'd\psi'}{(\sin^2\psi-\sin^2\psi')^{1/2}}. \tag{24}$$

The intensity profile for the full distribution is then derived by convolving $I_2(\psi)$ with the distribution Φ_2 about the y' axis:

$$I_1(\psi)=2\int_{-\pi/2}^{\pi/2}I_2(\psi'')\Phi_2[\cos(\psi-\psi'')]d\psi''=2I_2(\psi)*\Phi_2(\cos\psi). \tag{25}$$

6. Azimuthal sharpening

The sharpening procedure is a reversal of the above construction. (i) Solve the convolution equation (25) for $I_2(\psi)$ with

$$I_1(\psi)=I_{exp}(\psi) \tag{26}$$

and

$$\Phi_2(\cos\psi)=\frac{I_{eq}(\psi)}{2\int_{-\pi/2}^{\pi/2}I_{eq}(\psi)d\psi} \tag{27}$$

where $I_{exp}(\psi)$ is the experimental intensity profile at the given value of s, and $I_{eq}(\psi)$ is the intensity profile for an isolated equatorial arc.

The new azimuthal profiles $I_2(\psi)$ will build up a partially sharpened version of the diffraction pattern, in which the component of smearing due to the distribution of entity axes around the y' axis has been removed.

(ii) Solve equation (24) for $I(\psi')$ with

$$D_1(\psi)=\frac{(\cos\psi)I_{eq}(\psi)}{\int_{-\pi/2}^{\pi/2}(\cos\psi)I_{eq}(\psi)d\psi}. \tag{28}$$

When (24) has been solved, the equators of the fibre entities are aligned with the equator of the diffraction pattern and hence ψ' (measured from the equator of an entity) can be replaced by ψ (measured from equator of diffraction pattern). The fully sharpened pattern can then by synthesized from the functions $I(\psi)$.

Several techniques (Jones & Misell, 1970; Klug & Alexander, 1974) are available for the solution of (25) and (24). Fourier methods (Stokes, 1948) are applicable to (25) since it is a convolution. However, the integral (24) requires an iterative or matrix inversion approach. In this work an iterative approach (Burger & van Citter, 1932; Ergun, 1968) has been used to solve both equations as it is less sensitive to errors in the data than are inversion or even Fourier methods (Jones & Misell, 1970).

The convolution equation is written

$$f(x)=g(x)*h(x) \tag{29}$$

where $h(x)$ is the smearing function and $\int h(x)dx=1$, and deconvolution solves this for $g(x)$.

The iterative method evaluates successive approximations starting from $f(x)$:

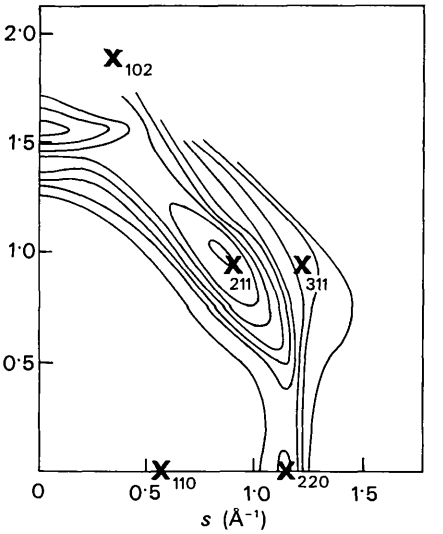

Fig. 8. Fully sharpened intensity pattern for aligned, glassy isotactic polystyrene. The crosses mark the positions of the most intense reflexions for aligned, crystalline isotactic polystyrene. Adapted from Lovell & Windle (1976).

$$g_0(x) = f(x)$$
$$g_1(x) = 2f(x) - f(x) * h(x)$$
$$\cdots\cdots\cdots\cdots\cdots\cdots\cdots\cdots\cdots\cdots$$
$$g_{n+1}(x) = g_n(x) + [f(x) - g_n(x) * h(x)] . \quad (30)$$

Iteration stops when the correction term, $f(x) - g_n(x) * h(x)$, is of the same order of magnitude as the errors in the original data.

For solving the more general equation (24), the convolution operation in (30) is replaced by the integral of (24).

The fully sharpened version of the data of Fig. 2 is shown in Fig. 8. The first equatorial halo is not plotted as it will of course have zero azimuthal spread. There is marked agreement with the crystalline fibre pattern.

7. Conclusions

The azimuthal sharpening technique described in this paper is particularly applicable where a well separated equatorial halo is available for determining the distribution of entity axes. In principle, a meridional halo would be even easier to use since it gives a section of the distribution directly. However, meridional reflexions are much more sensitive to disorder such as curved chains or lack of longitudinal register between the chains which will smear the reflexion along the layer line. This component of smearing would be difficult to remove.

The smearing process of § 5 could, in fact, be carried out in a single step for any form of $\Phi(\alpha_1, \alpha_2)$, although this would involve complicated double integrals. Thus the iterative method could be used to reverse the process in a single step. However, this requires knowledge of $\Phi(\alpha_1, \alpha_2)$ rather than its projection. For fibre symmetry, we would additionally need to solve (12) for Φ_2.

We acknowledge the stimulation of correspondence with Professor W. Ruland on this topic and also the financial support provided by the Science Research Council.

References

BURGER, H. C. & VAN CITTERT, P. H. (1932). *Z. Phys.* **79**, 722–730.
COLEBROOKE, A. & WINDLE, A. H. (1976). *J. Macromol. Sci. (B).* **12**, 373–382.
ERGUN, S. (1968). *J. Appl. Cryst.* **1**, 19–23.
JONES, A. F. & MISELL, D. L. (1970). *J. Phys. A: Gen. Phys.* **3**, 462–472.
KLUG, H. P. & ALEXANDER, L. E. (1974). *X-ray Diffraction Procedures for Polycrystalline and Amorphous Materials.* 2nd ed., pp. 618–633. New York: John Wiley.
LOVELL, R. & WINDLE, A. H. (1976). *Polymer*, **17**, 488–494.
STOKES, A. R. (1948). *Proc. Phys. Soc.* A **61**, 382–391.

Acta Cryst. (1977). A **33**, 395–398

Theoretical Approach to the Derivation of Condensed Models of Crystal Structures Based on Square-Type Layers

BY M. O. FIGUEIREDO AND J. LIMA-DE-FARIA

Junta de Investigações Científicas do Ultramar, Alameda D. Afonso Henriques, 41-4° E, Lisbon-1, Portugal

(*Received* 12 *November* 1976; *accepted* 14 *November* 1976)

Condensed models of crystal structures based on the stacking of equal square-type layers corresponding to the three possible symmetries (plane groups *p4m*, *p4g* and *p4*) are studied in a general way for the regular stacking modes. The minimum set of standard sheets required to represent any structure based on each layer symmetry is derived by considering transparent sheets, either square or standard rectangular in shape. In the latter case four sheets are necessary for *p4m* and *p4g* patterns, and eight sheets for *p4* patterns. An example of a *p4g* layer occurring in the $CuAl_2$ and TlSe structures is presented.

Introduction

The representation of crystal structures, which is a three-dimensional problem, can in most cases be formally decomposed into a $2D+1D$ (two-plus-one-dimensional) problem by considering sections of the structure (layers) and the way they stack together. Crystal-structure models can therefore be designed by slicing the structure into layers of atoms and drawing them on transparent sheets which are then mounted one above another with a proper spacing. Such models are particularly useful for representing inorganic close-packed structures and are called 'condensed models' (Lima-de-Faria, 1965, 1966). Standard sheets have been designed where the packing atoms are represented by full circles, and all the possible interstitial sites resulting from the stacking of the adjacent close-packed layer are drawn as dashed circles. Any layer of a close-packed structure is figured out simply by painting in the occupied interstitial sites, and in this way a versatile sys-